Structure of oxychloride glasses by neutron and x-ray 'difference' and x-ray photoelectron spectroscopy

2003 J. Phys.: Condens. Matter 15 4679

(http://iopscience.iop.org/0953-8984/15/27/303)

INSTITUTE OF PHYSICS PUBLISHING JOURNAL OF PHYSICS: CONDENSED MATTER

J. Phys.: Condens. Matter **15** (2003) 4679–4693 PII: S0953-8984(03)59343-2

Structure of oxychloride glasses by neutron and x-ray 'difference' and x-ray photoelectron spectroscopy

J A Johnson[1,5], D Holland[2], J Urquidi[3], I A Gee[2], C J Benmore[3] and C E Johnson[4]

[1] Energy Technology Division, Argonne National Laboratory, Argonne, IL 60439-4845, USA
[2] Physics Department, Warwick University, Coventry CV4 7AL, UK
[3] Intense Pulsed Neutron Source, Argonne National Laboratory, Argonne, IL 60439-4845, USA
[4] Physics Department, Northern Illinois University, DeKalb, IL 60115, USA

E-mail: jaj@anl.gov

Received 7 February 2003, in final form 2 June 2003
Published 27 June 2003
Online at stacks.iop.org/JPhysCM/15/4679

Abstract

A previous study of the binary system, $[Sb_2O_3]_x$–$[ZnCl_2]_{1-x}$ (Johnson *et al* 2003 *J. Phys.: Condens. Matter* **15** 755–64), where nominally $x = 0.25$, 0.50, 0.75 and 1.00, has been extended to include Sb_2O_3–$PbCl_2$. Information about the structure has been obtained from a combination of neutron and x-ray diffraction measurements, which were complemented by x-ray photoelectron spectroscopy. The data clearly show preferential bonding of oxygen to antimony and chlorine to zinc or lead in a single-phase glass with minimal change in the polyhedral structure with composition. The structure appears to be controlled by the need to avoid Sb–Cl–Sb links.

1. Introduction

The studies reported here were undertaken with the aim of establishing whether cations would exhibit preferred coordination when there was a choice of anion available in a glass. Most glasses contain a mixture of cations but rarely a mixture of anions. However, such glasses are of significant technical importance; oxynitrides represent the residual glass phase in engineering ceramics and mixed chalcogenide glasses and oxyhalide glasses are of relevance to optical applications. We have performed earlier studies on oxychloride glasses developed for IR transmission and as low phonon energy hosts for lasing ions [2, 3], and recently we have reported the results of a neutron diffraction study of the Sb_2O_3–$ZnCl_2$ system which indicated that preferential cation–anion associations do occur [1]. The interpretation of the neutron diffraction data required various assumptions to be made about coordination number because of the overlap of the metal–oxygen correlations and also overlap of the metal–chlorine

[5] Author to whom any correspondence should be addressed.

correlations. To extract information on the individual correlations would require costly isotope substitution so we have chosen instead to complement the neutron diffraction work with a further study using high energy x-ray diffraction. One advantage of x-rays is that the same sample can be studied as with neutrons. Also the different sensitivity of x-rays and neutrons to the various elements enables peaks to be uniquely resolved between the two spectra in many cases. Sometimes it is necessary to subtract the spectra in order to resolve the peaks, creating a 'difference' spectrum. In this way, neutron and x-ray combinations are useful in eliminating individual partial structure factors.

Of the glass components employed (Sb_2O_3, $SbCl_3$, $ZnCl_2$ and $PbCl_2$), Sb_2O_3 and $ZnCl_2$ are known to be glass formers though Sb_2O_3 is usually difficult to make as a single-component glass by conventional melt quenching and requires the addition of a second component, e.g. B_2O_3 [4]. The structure of Sb_2O_3 as determined by Hasegawa *et al* [4] with conventional x-ray diffraction gave an Sb–O separation of 1.99 Å and co-ordination of 3.15. The Sb–Sb separation obtained was 3.6 Å and they deduced an O–Sb–O bond angle of $\sim 92^\circ$ by assuming an O–O distance of 2.8 Å. They concluded that the glass was closest in structure to valentinite [5, 6], in which 4 [SbO_3] pyramids are linked to form rings. Masuda *et al* [7] failed to produce a single-component Sb_2O_3 glass but, using x-ray fluorescence, concluded that both Sb^{3+} and Sb^{5+} were present in binary antimonate glasses. Neutron diffraction of $ZnCl_2$ glass [8] was interpreted as consistent with $[ZnCl_4]^{2-}$ in which the Zn–Cl distance was 2.288 Å and both Cl–Cl and Zn–Zn distances were 3.72 Å. Of the remaining glass components, it is generally accepted that PbO enters glasses to give [PbO_3] and [PbO_4] polyhedra [9] and ZnO gives [ZnO_4] tetrahedra in situations where it is acting as an intermediate and taking part in forming the glass network [10]. The environments of the halides are not well characterized but examination of the crystal structures would suggest the likely formation of [$SbCl_3$] and [$PbCl_3$] or [$PbCl_4$] pyramids.

X-ray photoelectron spectroscopy (XPS) provides a means of examining the chemical environments of individual elements and has been particularly effective in the study of bridging/non-bridging oxygen distribution in glasses [11]. The technique has been used extensively on oxide glasses but there is little in the literature on halide glasses. Kadono *et al* [12] performed XPS on glassy $ZnCl_2$ and $(60-x)ZnCl_2{\cdot}40CsCl{\cdot}xBaCl_2$ glasses. They obtained a Cl $2p_{3/2}$ binding energy of 200.0 eV for pure $ZnCl_2$ but this value decreased to 199.2 eV on addition of CsCl and $BaCl_2$ and resulted in the formation of non-bridging Cl. Montagne *et al* [13], using NMR and XPS of a $PbO–PbCl_2–CdCl_2$ system, assigned the three peaks which they observed in the O 1s spectrum to Pb–O–Pb (531.0 eV) OH (532.9 eV) and Pb–O–Cd or Cd–O–Cd (529.8 eV).

2. Experimental details

2.1. Glass preparation

Glass preparation details have been reported elsewhere [1]. X-ray diffraction was used to check the amorphicity of the glasses and density was determined using an autopycnometer. Since chlorine is lost from the glasses by hydrolysis and oxidation during melting, their actual compositions were determined by wet chemical analysis by the Analytical Chemistry group at Argonne National Laboratory (ANL). Analysis was performed for the cations and for oxygen and the chlorine content was obtained by difference. Interestingly, there was no calculable chlorine in the nominal $0.5Sb_2O_3–0.5SbCl_3$ sample. This indicated that the sample must be close to v-Sb_2O_3, which turned out to be a convenient base glass for these measurements. There was no detectable contamination from the alumina crucible.

2.2. Diffraction

Pulsed neutron diffraction measurements were made on GLAD (Glass, Liquids and Amorphous Materials Diffractometer) at IPNS (the Intense Pulsed Neutron Source) at ANL. Neutron data analysis was performed using the ATLAS suite of programs [14]. X-ray measurements were performed on the high-energy beam line 11-ID-C at the Advanced Photon Source (APS) at ANL using an energy of 115 keV; these counts were corrected using the ISOMER-X program [15]. Data were collected using momentum transfers (Q) from 0.3 up to 40 Å^{-1} and, after analysis, yielded the static structure factor, $S(Q)$:

$$S(Q) - 1 = \frac{I(Q)}{[\sum_i c_i W_i(Q)]^2} = \frac{\sum_{ij} c_i W_i(Q) c_j W_j(Q)(S_{ij}(Q) - 1)}{[\sum_i c_i W_i(Q)]^2}, \tag{1}$$

where c_i is the concentration of species i and W_i is the coherent scattering length, b_i for neutrons and the atomic form factor for x-rays.

The measured neutron and x-ray $S(Q)$ are related to the total radial distribution function $G(r)$ via a Fourier transform, given by

$$S(Q) = 1 + \frac{4\pi\rho}{Q} \int_0^\infty r \, \mathrm{d}r \, (G(r) - 1) \sin(Qr), \tag{2}$$

where ρ is the atomic number density.

Typical results were plotted in terms of the total correlation functions:

$$T(r) = 4\pi\rho r G(r). \tag{3}$$

A Lorch modification function was used to reduce termination effects associated with the cut-off at Q_{max}, which in this case is 30 Å^{-1} for the neutron data and 18 Å^{-1} for the x-ray data. Statistical accuracy degrades with increasing Q due to the decreasing detector solid-angle coverage in the neutron experiments and the effect of the form factor for the x-ray experiments. However, truncating the data at lower Q values can introduce Fourier ripples, particularly at lower values, which overlap with the pair correlation functions.

2.3. XPS

XPS experiments were carried out on samples containing nominal 50 mol% $ZnCl_2$ and 25 and 50 mol% $PbCl_2$ using a Scienta ESCA 300 spectrometer at the Research Unit for Surfaces, Transforms and Interfaces (RUSTI), Daresbury Laboratory, UK. Photoelectron spectra were obtained from the O 1s, Cl 2p, Sb 3d, Zn 2p, Pb 4f and C 1s core levels, and Auger electron spectra from the Zn $L_3M_{4,5}M_{4,5}$, using monochromated Al Kα radiation (1486.6 eV) from a rotating anode source operated at 3 kW. The concentric hemispherical electron energy analyser (CHA) was operated with a pass energy of 50 eV and a step energy of 0.05 eV for high resolution XPS studies (the total theoretical energy resolution is approximately 350 meV) and 150 eV pass energy with a step of 1 eV for routine survey scan spectra. An electron flood gun, operating at 2–3 eV, was used to reduce the effects of surface charging which are significant when studying predominantly insulating surfaces. Since the effects cannot be fully compensated, all binding energies were referenced to either the adventitious C 1s peak at 284.5 eV (bulk samples) or to the C 1s peak at 285 eV arising from the carbon sticky pad (powder samples).

Sample size prevented the generation of *in situ* fracture and therefore XPS was performed on flat bulk surfaces mounted on the surface of adhesive carbon pads. Some measurements were similarly performed on related crystalline oxides and chlorides in powder form. All of the spectra presented in this paper show the as-collected (unsmoothed) data, with a Shirley background subtraction [16] being the only processing performed on each spectrum.

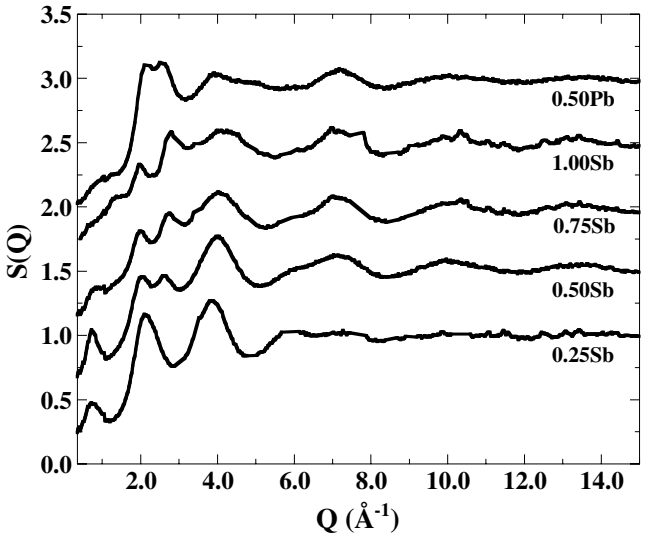

Figure 1. Neutron structure factors $S(Q)$ for oxychloride glasses containing nominally 0.25, 0.50, 0.75 and 1.00 mol fraction of Sb_2O_3 and 0.50 mol fraction of $PbCl_2$. Successive curves are displaced vertically by 0.5 for clarity.

Table 1. Densities and nominal and analysed compositions (atom%) for the glasses studied (estimated accuracy ±5% of value: repeated measurements agreed to within this value).

Sample	Density (g cm^{-3})	Sb		Pb		Zn		O		CI	
		Nom	An	Nom	An	Nom	An	Nom	An	Nom	An
1.00Sb	5.05	33.3	40.6	—	—	—	—	33.3	59.4	33.3	0.0
0.75Sb	4.76	33.3	36.2	—	—	5.5	5.6	50.0	53.6	11.0	4.6
0.50Sb	4.60	25.0	27.9	—	—	12.5	12.9	37.5	48.8	25.0	10.4
0.25Sb	3.92	14.3	15.7	—	—	21.4	22.1	21.4	34.0	42.9	28.1
0.50Pb	5.48	25.0	25.6	12.5	12.3	—	—	37.5	39.5	25.0	22.6

3. Results

Table 1 gives the densities and the nominal and analysed compositions of the glasses examined. The compositions are given in atomic% in order to allow comparison of the losses occurring during melting. X-ray diffraction confirmed the glassy nature of the samples and ^{121}Sb Mössbauer spectroscopy confirmed that antimony was present in the trivalent Sb^{3+} state only [1].

Figure 1 shows the neutron diffraction structure factors, $S(Q)$; the spectra are displaced by 0.5 for clarity. They are only shown out to 15 Å^{-1} as the spectra show no features beyond this. The 0.25Sb sample, which contained the most chlorine, had to undergo an additional absorption correction, larger than the nominally calculated value obtained from the ATLAS package by a factor of 4. The typical random error on $S(Q)$ for the neutron data range from 1% at 2 Å^{-1} to 5% at 30 Å^{-1}. Figure 2 shows the corresponding data for x-ray diffraction structure factors displaced by 1.5. Typical errors here range from 1% at 2 Å^{-1} to 8% at 18 Å^{-1}.

The first sharp diffraction peak (FSDP) occurs at a wavevector Q_1 and gives information on the intermediate-range-order (IRO) length scale [17]. The occurrence of this peak in v-$ZnCl_2$ is thought to be due to *voids* in the spatial distribution of cations [18]. The weak

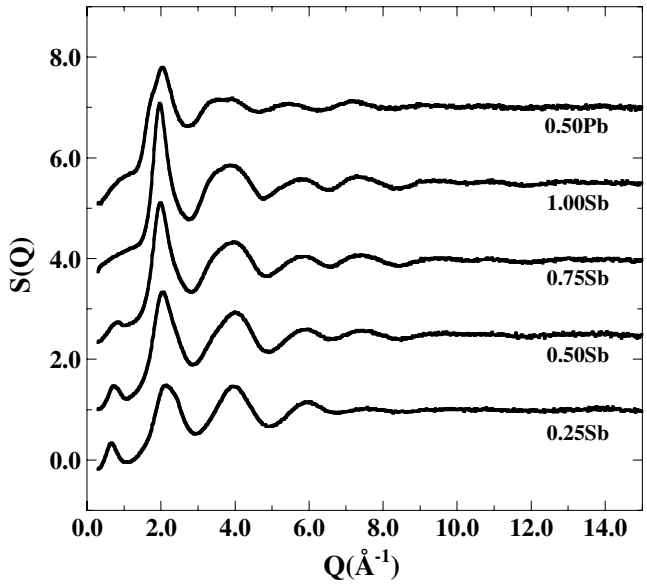

Figure 2. X-ray structure factors $S(Q)$ for oxychloride glasses containing nominally 0.25, 0.50, 0.75 and 1.00 mol fraction of Sb_2O_3 and 0.50 mol fraction of $PbCl_2$. Successive curves are displaced vertically by 1.5 for clarity.

Table 2. Positions of the FSDP, EROP and implied repeat distances for neutrons, with x-ray data in parentheses.

Sample	Q_0 (Å^{-1}) ±0.02	$2\pi/Q_0$ (Å) ±0.01	Q_1 (Å^{-1}) ±0.02	$2\pi/Q_1$ (Å) ±0.01
1.00Sb	—	—	1.97 (1.96)	3.19 (3.21)
0.75Sb	0.77 (0.79)	8.16 (7.95)	1.97 (1.98)	3.19 (3.17)
0.50Sb	0.73 (0.72)	8.61 (8.73)	2.01 (2.03)	3.13 (3.10)
0.25Sb	0.71 (0.65)	8.85 (9.67)	2.11 (2.11)	2.98 (2.98)
0.50Pb	—	—	2.09 (2.03)	3.01 (3.10)

ordering of these voids tends to induce cation density fluctuations, with a layered character giving a well-defined IRO network. The Sb_2O_3-rich glasses have a less well-defined network and so the FSDP decreases as Sb is added in both the x-ray and neutron data. On the addition of antimony the peak also shifts to lower Q. Since the FSDP corresponds to oscillations with periodicity $2\pi/Q$ in real space, this implies an increase in the separation of the structures contributing to the IRO correlations. The samples containing $ZnCl_2$ also have an extended-range-order peak (EROP) at Q_0. It is clear that the IRO is most significant in these glasses. Table 2 shows the positions of the resolvable FSDPs and EROP. The numbers in parentheses relate to the x-ray data. Within error the majority of the values are the same for both the x-ray and neutron data, the exceptions being Q_1 in the lead–antimony sample and Q_0 in the 0.25Sb sample. The reason for this is likely to be the different sensitivities of the neutron and x-ray probes to the elements which are controlling the extended order.

Figures 3 and 4 show the real space $T(r)$ function for the series of glasses along with the peak assignments. The statistical errors on $T(r)$ were calculated using the method of Weitkamp *et al* [19] and were found to be less than 1% throughout the range of r for all spectra.

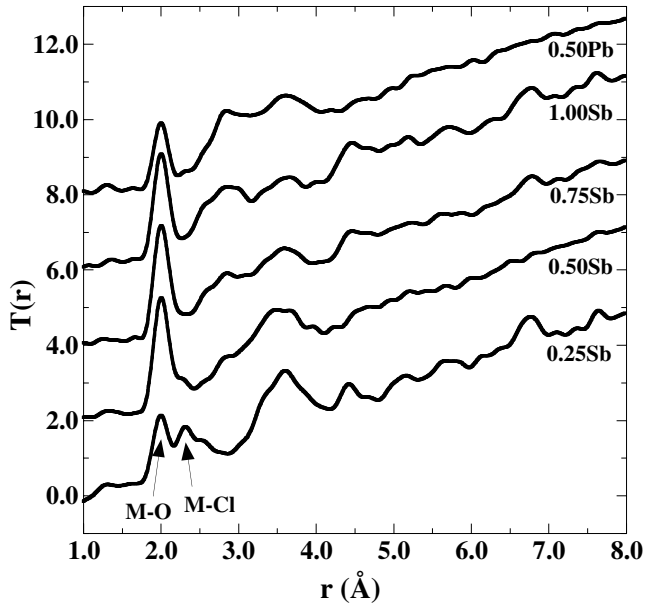

Figure 3. Neutron correlation functions, $T(r)$, for oxychloride glasses of figure 1. Successive curves are displaced vertically by 2.0 for clarity.

The resolution for neutrons is much higher due to being able to get reliable data out to 30 $Å^{-1}$, compared with 18 $Å^{-1}$ for x-rays. The different sensitivities of the elements to the neutrons and x-rays are clear in these figures: x-rays are most sensitive to Pb and Sb, as they are heavy elements, and not so sensitive to O, Cl and Zn. Neutrons, however are sensitive to oxygen containing correlations. This makes the task of assigning peaks a simpler job. The distinguishable peaks were fitted with deconvoluted Gaussians (representative fits have been previously shown [1]) from which the peak positions and co-ordination numbers are derived. These are summarized in table 3.

XPS spectra from the Cl 2p and O 1s core levels are shown in figures 5–7, respectively.

4. Discussion

4.1. Glass composition

Table 1 shows that there is significant loss of chlorine from the glasses, with the proportion lost decreasing as the total chlorine increases. Relative to Sb, some Zn is lost from the glasses at lower concentrations of Zn; the Sb/Zn ratio deviates from the nominal by 8% for the 0.75 Sb_2O_3 glass but by less than 1% for the 0.25 Sb_2O_3 glass. The change in the glass density with composition is consistent with replacement of Sb_2O_3 (MW = 291.5) by $ZnCl_2$ (MW = 136.3) and is enhanced by loss of Cl. The $PbCl_2$-containing glass is far more resistant to hydrolysis and 90% of the Cl is retained.

4.2. Diffraction

The observed peak positions, reported in table 3, are compared with inter-atomic distances observed for v-Sb_2O_3 [4], v-$ZnCl_2$ [8], valentinite [6], c-$ZnCl_2$ [20], c-ZnO [21], c-$SbCl_3$ [22], v-PbO/$PbCl_2$ [23], c-PbO red [24], c-PbO yellow [25], c-$PbCl_2$ [26] and c-$Pb_3O_2Cl_2$ [27] and

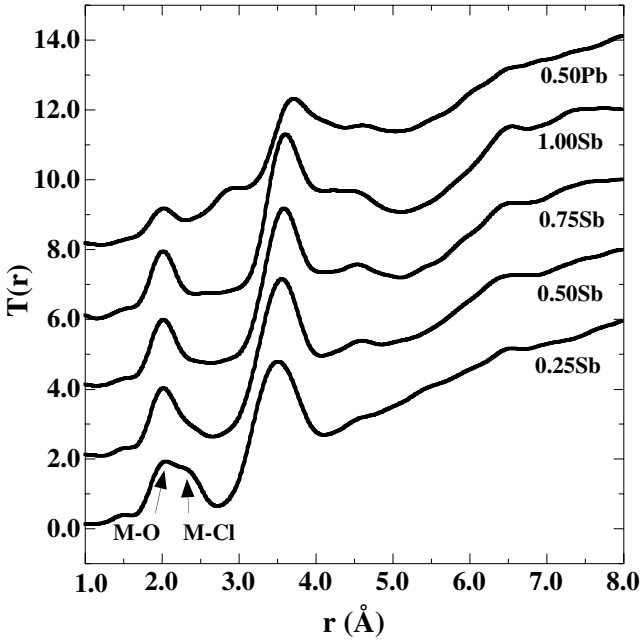

Figure 4. X-ray correlation functions, $T(r)$, for oxychloride glasses of figure 2. Successive curves are displaced vertically by 2.0 for clarity.

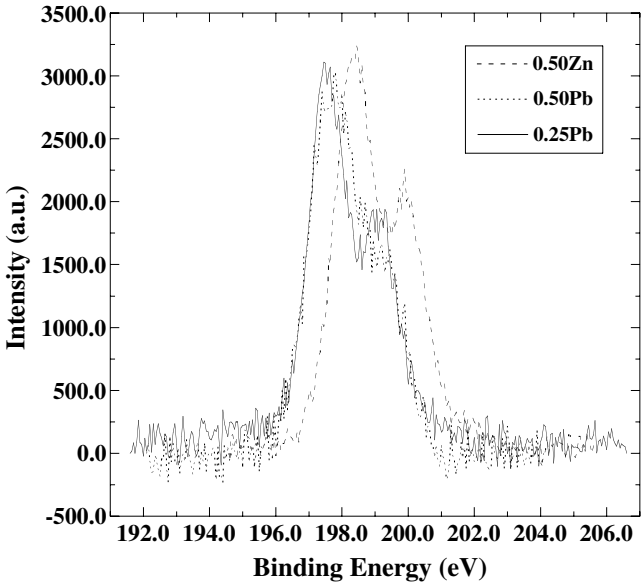

Figure 5. Cl $2p_{3/2}$ photoelectron spectra for $PbCl_2$-and $ZnCl_2$-containing glasses.

also the distances calculated from bond valence parameters [28]. Our previous work [1] reported the peak at ∼2.0 Å as arising from metal–oxygen correlations and the peak at ∼2.3 Å from metal–chlorine correlations for the zinc containing samples. The similar

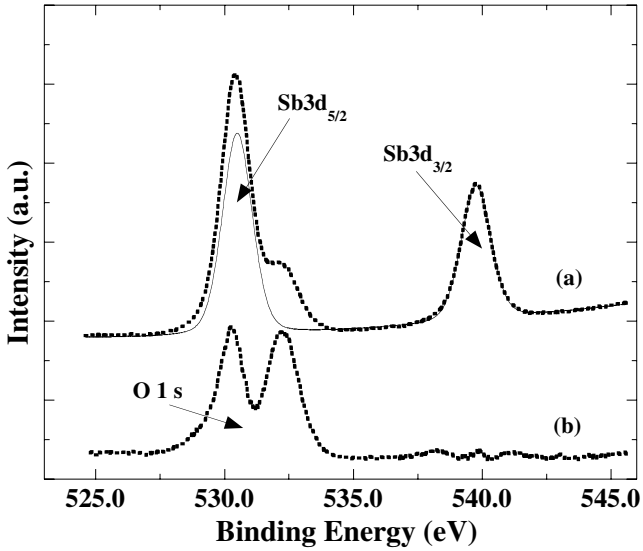

Figure 6. (a) Photoelectron spectrum from Sb 3d and O 1s. (b) O 1s residual after removal of Sb 3d (×2 for clarity).

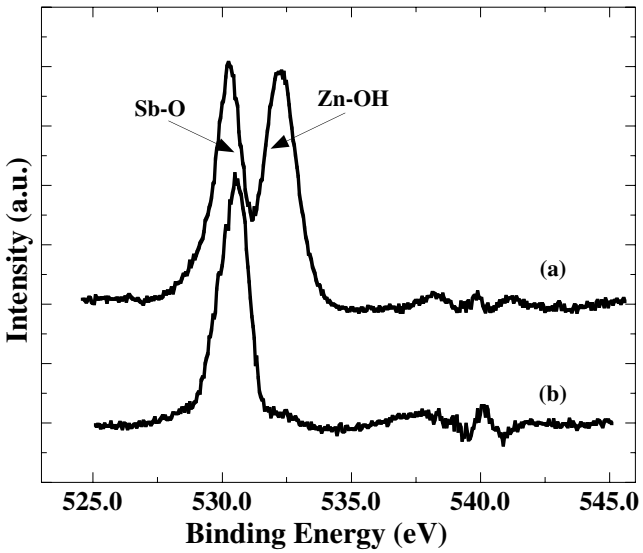

Figure 7. Photoelectron spectrum from O 1s for (a) 0.50Sb and (b) 0.50Pb sample after Sb 3d removal.

scattering lengths of Sb and Zn (Sb 5.57 fm, Zn 5.68 fm) were utilized to calculate the preferred co-ordinations of the cations. The results were consistent with co-ordinations of 3 and 4 for Sb and Zn, respectively. The Pb-containing sample is somewhat different as the oxide and chloride peaks do not have the same bond length for Sb and Pb.

The real-space correlation function from the 0.50Pb sample was fitted with four peaks at 1.997, 2.350, 2.610 and 2.830 Å. The peak positions' height and widths in the Gaussian fitting program were iterated by hand until the best fit was obtained, for the last three peaks, due to

Table 3. Observed inter-atomic separations and co-ordination numbers compared with values from the literature.

Sample	R_{M-O} (Å ± 0.005)	R_{M-Cl} (Å ± 0.005)	C_{M-O} ± 0.2	C_{M-Cl} ± 0.2
1.00Sb	1.997		2.1	
0.75Sb	2.006		2.5	
0.50Sb	2.001	2.307	3.5	2.6
0.25Sb	1.985	2.320	5.0	2.5
0.50Pb	1.997 (Sb–O)	2.35 (Sb–Cl)	2.9	
	2.350 (Pb–O)	2.61 (Pb–Cl)		
		2.83 (Pb–Cl)		
Bond valence	Zn–O 1.960	Zn–Cl 2.266	4.0	4.0
calculation [27]	Sb–O 1.973	Sb–Cl 2.350	3.0	3.0
	Pb–O 2.262	Pb–Cl 2.680	3.0	3.0
	Pb–O 2.368	Pb–Cl 2.786	4.0	4.0
v-$ZnCl_2$ [8]		2.288		3.8
v-Sb_2O_3 [4]	1.990		3.2	
c-$ZnCl_2$ [19]		av 2.273		4.0
c-Sb_2O_3 [6]	2.000		3.0	
c-ZnO [20]	1.974		4.0	
c-$SbCl_3$ [21]		av 2.360		3.0
v-PbO/$PbCl_2$ [22]	2.22	3.000		PbO_2Cl_4
c-PbO red [23]	2.30		4	
c-PbO yellow [24]	2.215, 2.490		2 + 2	
c-$PbCl_2$ [25]		2.67–3.29		Approx 7–9
c-$Pb_3O_2Cl_2$ [26]	2.33	3.12–3.44	2	4
3 Pb positions	2.33	2.95–3.44	4	3
	2.33	2.93–3.21	2	5

the overlap. The inter-atomic distances obtained from the bond valence calculations are listed in table 3 and peak assignments could be as follows: 1.997 Å, Sb–O (3 CN) consistent with v-Sb_2O_3, 2.35 Å, Sb–Cl (3 CN) and/or Pb–O (4 CN), 2.61 Å, Pb–Cl (3 CN) and 2.83 Å, Pb–Cl (4 CN) and/or O–O.

Rao *et al* [22], studying PbO–$PbCl_2$ glasses claimed that Pb is octahedrally coordinated with 2 O at 2.25–2.35 Å and 4 Cl at 2.75–2.85 Å.

The complementary x-ray data and difference calculations can help to clarify the results.

The neutron and x-ray structure factors represent different combinations of partial structure factors $S_{ij}(Q)$, where the indices i and j refer to the atom type. In a system with n components there are $n(n+1)/2$ partial structure factors. Table 4(a) gives the weights of the partial structure factors for Sb_2O_3.

It is immediately obvious that x-rays are comparatively insensitive to oxygen and if we look at the x-ray spectrum in figure 8 we can see that all the intensity between 2.5 and 3 Å disappears in comparison to the neutron spectrum. We know from previous data that Sb–O has a peak around 2 Å: this is clear in both spectra. From the x-ray data we can clearly attribute the peak at 3.6 Å to Sb–Sb. The connectivity of Sb polyhedra may give a significant contribution to the FSDP. There are peaks in the neutron data at 2.6, 2.8 and 3.0 Å: these are most likely to be O–O of varying bond lengths since they do not appear in the x-ray data. This suggests that either a variety of M–O polyhedra exist or they are distorted in these samples, especially in the 1.00Sb sample (figure 8). We can now use this information in the other compositions.

Table 4. The weights of partial structure factors at $Q = 0$.

(a) 1.00Sb sample			
ij		$W_N(ij)$	$W_X(ij)$
Sb–Sb		0.157	0.662
O–O		0.365	0.035
Sb–O		0.479	0.304
(b) 0.50Sb sample			
ij	$W_N(ij)$	$W_X(ij)$	Δ
Sb–Sb	0.065	0.358	0.380
Zn–Zn	0.014	0.027	0.018
O–O	0.214	0.027	−0.190
Cl–Cl	0.026	0.006	−0.021
Sb–Zn	0.061	0.195	0.180
Sb–O	0.235	0.197	0.000
Sb–Cl	0.083	0.089	0.025
Zn–O	0.111	0.053	−0.049
Zn–Cl	0.039	0.024	−0.011
O–Cl	0.151	0.024	−0.127
(c) 0.50Pb sample			
ij	$W_N(ij)$	$W_X(ij)$	Δ
Sb–Sb	0.041	0.188	0.190
Pb–Pb	0.027	0.112	0.111
O–O	0.106	0.011	−0.097
Cl–Cl	0.094	0.016	−0.079
Sb–Pb	0.067	0.290	0.290
Sb–O	0.132	0.091	−0.026
Sb–Cl	0.125	0.110	0.007
Pb–O	0.107	0.070	−0.025
Pb–Cl	0.101	0.085	0.000
O–Cl	0.200	0.027	−0.176

In the 0.50Sb sample there are four components and therefore ten partial structure factors, the weightings of which are given in table 4(b). This shows that the x-rays are going to be most sensitive to Sb–Sb, Sb–Zn, Sb–O and, to a lesser extent, Sb–Cl. This is certainly clear in figure 9. Neutrons are most sensitive to Sb–O and O–O and, with a non-negligible weight, also to O–Cl. The same O–O peaks show in the neutron data here as in figure 8. There is a small peak in the neutron data at 2.3 Å which we have previously attributed to Zn–Cl interactions. There is some intensity in the x-ray spectrum but it is not so clear as it is for neutrons.

Having made two independent measurements, neutron and x-ray diffraction, we can eliminate partials one at a time to calculate the 'difference' structure factors using the following relation:

$$\Delta S(Q) = \frac{S_N(Q) - (W_N/W_X(Q))S_X(Q)}{1 - (W_N/W_X(Q))}. \tag{4}$$

In sample 0.50Sb, it was decided to eliminate the Sb–O partial structure factor to give a clearer picture of the O–O interaction. The difference is calculated in Q-space to account for the Q-dependent x-ray form factors and to avoid inaccuracies due to the different resolutions in real space. The Fourier transform was subsequently done on the Q-space *difference* spectrum

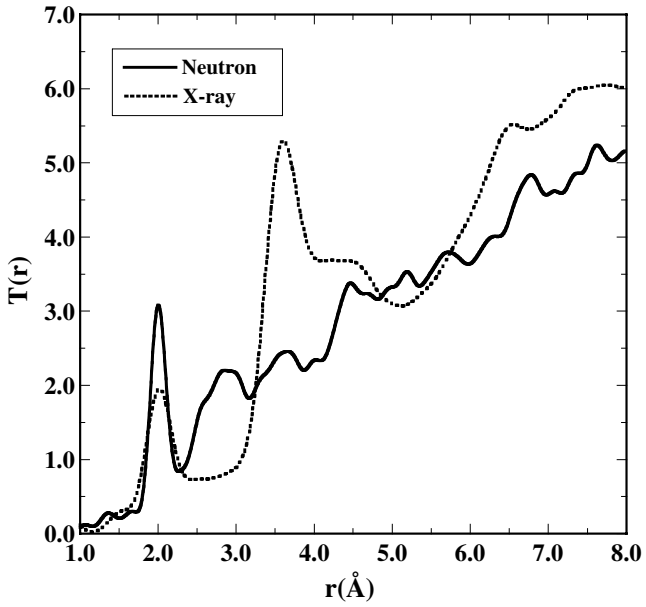

Figure 8. Neutron and x-ray data for 1.00Sb sample.

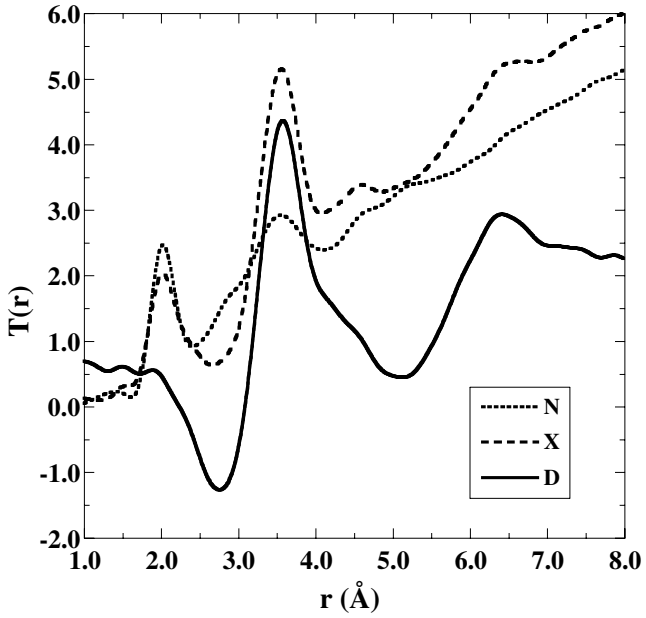

Figure 9. Neutron, x-ray and difference data (SbO eliminated) for the 0.50Sb sample. The difference data is scaled by 0.5 for clarity.

to obtain the *difference* in real space. The *difference* weighting factors after this elimination are also shown in table 4(b). While the Sb–Sb interaction remains strong and very clear in figure 9, the O–O interaction is enhanced and negative and appears as a broad peak at 2.7 Å.

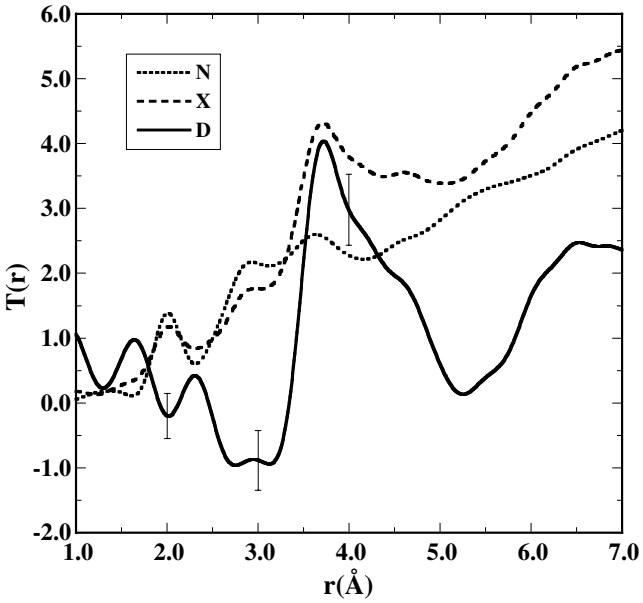

Figure 10. Neutron, x-ray and difference data (PbCl eliminated) for the 0.50Pb sample with selected error bars. The difference data are scaled by 0.5 for clarity.

The *difference* spectrum in figure 9 has been scaled by 0.5 for clarity and the neutron data has been cut at 18 $Å^{-1}$ so that a direct comparison of spectra can be made. Table 4(c) shows the weighting factors for the 0.50Pb sample. In this sample there is possible overlap of the Sb–Cl and Pb–O peaks and the Pb–Cl and O–O peaks. Looking at the weighting factors we can see that the sensitivity of x-rays to the O–O peak is an order of magnitude less than that of neutrons so we can see from figure 10 (difference spectrum also scaled by 0.5 and neutron data cut at 18 $Å^{-1}$) that, since there is intensity at 2.8 Å, it is most likely to be Pb–Cl. The weighting factors are roughly the same for Pb–Cl for neutrons and x-rays so the fact that the neutron data show a more intense peak at 2.8 Å than the x-ray data implies there is both O–O and Pb–Cl at this position. The best way to clarify this is to eliminate the Pb–Cl, as can be seen from the resulting 'difference' weighting factors shown in table 4(c). The table clearly shows that the difference spectrum is going to be dominated by the M–M interaction. There is a clear peak and two shoulders at 3.7, 4.2 and 4.6 Å, respectively. Due to the size of the atoms, and deducing from figure 8, these are likely to be, Sb–Sb, Sb–Pb and Pb–Pb, in order of increasing bond length. The significant negative peaks are going to be O–O, O–Cl and Cl–Cl interactions. In figure 9, we see one negative peak at 2.7 Å, which, from table 4(b), we can assume is a mixture of O–O and O–Cl, as Cl–Cl has no significant intensity. The implication is that the negative peak around 3.1 Å in figure 10 is due to Cl–Cl interactions.

Due to the fact that the M–O and M–Cl interactions all have similar weightings for both x-ray and neutrons, when we eliminate the Pb–Cl, we essentially eliminate Sb–O, Pb–O and Sb–Cl as well. It is also difficult to say whether the peak at 2.3 Å is real as the systematic errors are compounded in the difference spectra. Selected error bars are shown in figure 10; these are comparable to the size of the peak and so an unequivocal determination of the existence of Pb–O, Sb–Cl or both is not possible from this data.

To achieve a single-phase glass there must be some Pb–O–Sb and Pb–Cl–Sb bonds to link the networks. There was no visible light scattering in these glasses, indicating that there

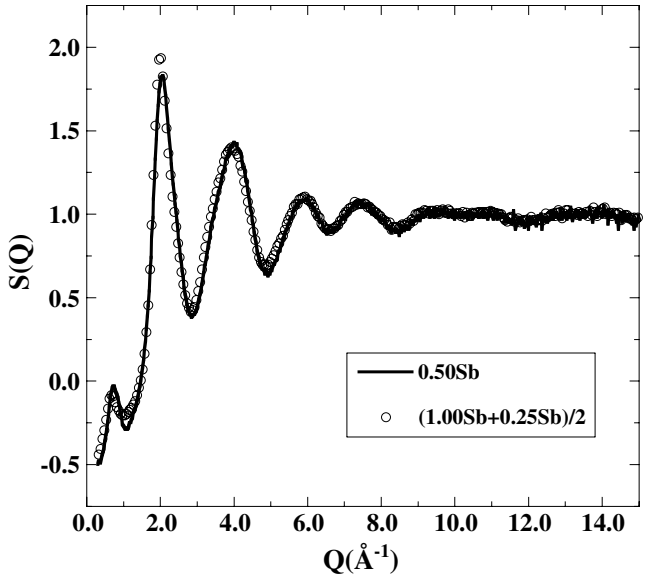

Figure 11. $S(Q)$ for the linear combination of the 1.00Sb and 0.25Sb glasses compared to the 0.50Sb glass.

is no phase separation on the hundreds of nanometres scale. Nor were two glass transitions observed from DTA. This, and the fact that there is no significant small-angle scattering (see figures 1 and 2 and [29]) suggests that the glasses are single phase. Another way to test this is to see if a linear combination of an Sb_2O_3-rich glass and a $ZnCl_2$-rich glass resembles the structure of an intermediate glass or gives a completely different picture. Summing the $S(Q)$'s of the 1.00Sb and 0.25Sb glasses and dividing by 2 fortuitously gives a composition close to the 0.50Sb glass. Figure 11 shows the comparison of this sum and the intermediate glass. The similarity is remarkable and strongly suggests that either there *are* minimal interactions between the two components (implying phase separation) or the structure does not need to alter much to accommodate the mixing of the $[SbX_3]$ and $[PbX_3]/[PbX_4]$ or $[ZnX_4]$ polyhedra.

4.3. XPS

Figure 5 shows the Cl 2p photoelectron spectra. The peaks exhibit a constant spin–orbit splitting of 1.6 ± 0.1 eV and the $2p_{3/2}$ peak from the samples containing Pb occurs at 197.6 ± 0.1 eV, whereas that from the Zn-containing sample occurs at 198.3 ± 0.1 eV. There is limited information in the literature on the Cl $2p_{3/2}$ binding energy in both glasses and crystals. Measurements performed as part of this study gave a binding energy of 198.6 ± 0.1 eV for c-$PbCl_2$ whereas c-$ZnCl_2$ gave two peaks of equal intensity at 199.5 ± 0.1 and 200.8 ± 0.1 eV. These values are shifted from those in the glasses by about 1 eV, which may be partly due to the different shift references used for the bulk samples and the powders. However, they are separated by a similar amount and in the same sense. This difference between the two systems indicates that chlorine is bonded to predominantly Pb or Zn in these glasses and not to Sb, which would lead to greater coincidence of the Cl 2p peaks.

The O 1s and Sb $3d_{5/2}$ photoelectron peaks overlap but can be separated as shown in figure 6 for the 50 mol% $ZnCl_2$ sample. The Sb $3d_{3/2}$ peak is first fitted and then a Sb $3d_{5/2}$ peak is generated at the correct separation, with the same half-width and with an intensity which

is 1.5 times that of the $3d_{3/2}$ peak. This can then be subtracted from the observed spectrum to leave a residual due to the O 1s only. The results of this subtraction for the 50% $PbCl_2$ sample and the 50% $ZnCl_2$ samples are shown in figure 7. The peaks at 530.3 ± 0.1 eV (50 $ZnCl_2$) and 530.5 ± 0.1 eV ($PbCl_2$) are due to oxygen bonded to Sb, whilst that at 532.2 ± 0.1 eV is due to OH (probably Zn–OH). As these are as-loaded samples the hydroxyl is likely to arise from hydrolysis of Cl sites near the surface. The O 1s binding energy obtained from Sb_2O_3 powder was 530.5 ± 0.1 eV. It is notable that little surface hydrolysis occurs for the $PbCl_2$-containing glass.

5. Conclusions

This paper reinforces the conclusions from our previous work using neutron scattering, and Mössbauer and Raman spectroscopy, in that the data clearly show that there is preferential bonding within the system with no evidence for Sb–Cl bonds. Further evidence for this is furnished by XPS, where the replacement of $ZnCl_2$ by $PbCl_2$ has a significant effect on the binding energy of the Cl $2p_{3/2}$ core level. The difference would be less pronounced if a significant fraction of the Cl were bonded to Sb. A linear combination of the end point structure factors reproduces the structure of an intermediate sample with slight differences in the low-Q region. This implies that the local environments, [ZnX_4] and [PbX_4] tetrahedra and [SbX_3] and [PbX_3] trigonal pyramids, do not need to change much to accommodate the mixing.

The results give the expected value for co-ordination of 3 O around Sb and 4 (O + Cl) around Zn. The structure is dictated by the avoidance of the formation of energetically unfavourable Zn–Cl–Sb and Sb–Cl–Sb linkages in the network.

Acknowledgments

Work at Argonne National Laboratory was supported by the US Department of Energy, Division of Material Sciences, Office of Basic Energy Sciences, under contract W-31-109-ENG-38. Access to the RUSTI facility at Daresbury Laboratory was provided by the Engineering and Physical Sciences Research Council of the UK and we are grateful for the help provided by Drs D S-L Law and G Beamson.

References

[1] Johnson J A, Holland D, Bland J, Johnson C E and Thomas M F 2003 *J. Phys.: Condens. Matter* **15** 755–64
[2] Ahmed M M and Holland D 1987 *Glass Technol.* **28** 141–4
[3] Sahar M R, Ahmed M M and Holland D 1990 *Phys. Chem. Glasses* **31** 126–31
[4] Hasegawa H, Stone M and Imaoka M 1978 *Phys. Chem. Glasses* **19** 28–33
[5] Buerger M J and Hendricks S B 1938 *Z. Kristallogr. Kristallgeom.* **98** 1
[6] Svensson C 1974 *Acta. Crystallogr.* B **30** 458
[7] Masuda H, Ohta Y and Morinaga K 1995 *Nippon Kinzoku Gakkaishi* **59** 31–6
[8] Desa J A E, Wright A C, Wong J and Sinclair R N 1982 *J. Non-Cryst. Solids* **51** 57
[9] Fayon F, Bessada C, Douy A and Massiot D 1999 *J. Magn. Reson.* **136** 116
[10] Lusvardi G, Malavasi G, Menabue L and Menziani M C 2002 *J. Phys. Chem.* B **106** 9753
[11] Holland D, Gee I A, Mekki A and McConville C F 2001 *Phys. Chem. Glasses* **42** 247–54
[12] Kadono K, Kinugawa K and Tanaka H 1994 *Phys. Chem. Glasses* **35** 59
[13] Montagne L, Donze S, Palavit G, Boivin J C, Fayon F, Massiot D, Grimblot J and Gengembre L 2002 *J. Non-Cryst. Solids* **293–295** 74
[14] Soper A K, Howells W S and Hannon A C 1989 ATLAS–Analysis of Time of flight diffraction data from Liquid and Amorphous Samples *Report* RAL 89-046, Rutherford Appleton Laboratory
[15] Urquidi J, Benmore C J, Neuefeind J and Tomberli B 2003 *J. Appl. Crystallogr.* **36** 368

[16] Shirley D A 1972 *Phys. Rev.* B **5** 4709
[17] Price D L, Moss S C, Reijers R, Saboungi M L and Susman S 1989 *J. Phys.: Condens. Matter* **1** 1005
[18] Wilson M and Madden P A 1998 *Phys. Rev. Lett.* **80** 532
[19] Weitkamp T, Neuefeind J, Fischer H E and Zeidler M D 2000 *Mol. Phys.* **98** 125
[20] Brynestad J and Yakel H L 1978 *Inorg. Chem.* **17** 1376
[21] Bragg W 1969 *Acta Crystallogr.* B **25** 123
[22] Lipka 1979 *Acta Crystallogr.* B **35** 3020
[23] Rao B G and Rao K J 1984 *Phys. Chem. Glasses* **25** 11
[24] Dickens B 1965 *J. Inorg. Nucl. Chem.* **27** 1503
[25] Dickens B 1965 *J. Inorg. Nucl. Chem.* **27** 1495
[26] Wyckoff R W G 1963 *Crystal Structures* vol 1 (New York: Wiley) p 298
[27] Gabrielson O 1957 *Ark. Miner. Geol.* **2** 29
[28] Brese N E and O'Keeffe M 1991 *Acta. Crystallogr.* B **47** 192
[29] Leheny R L, Menon N, Nagel S R, Price D L, Suzuya K and Thiyagarajan P 1996 *J. Chem. Phys.* **105** 17